

## Capacity Improvement of Tin-Deposited on Carbon-Coated Graphite Anode for Rechargeable Lithium Ion Batteries

*In-Tae Kim<sup>1</sup>, Jaeho Lee<sup>1,3</sup>, Jung-Chun An<sup>2</sup>, Euney Jung<sup>4</sup>, Hong-Ki Lee<sup>5</sup>, Masayuki Morita<sup>1,\*</sup>, Joongpyo Shim<sup>3,\*</sup>*

<sup>1</sup> Graduate School of Science and Engineering, Yamaguchi University, Ube, 755-8611, Japan

<sup>2</sup> Research Institute of Industrial Science & Technology, Pohang, Gyeongbuk 37673, Korea

<sup>3</sup> Department of Nano & Chemical Engineering, Kunsan National University, Jeonbuk, 54150, Korea

<sup>4</sup> Ruby Co., Ltd., Wanju-gun, Jeonbuk, 55319, Korea

<sup>5</sup> Fuel Cell Regional Innovation Center, Woosuk University, Jeonbuk, 55319, Korea

\*E-mail: [morita@yamaguchi-u.ac.jp](mailto:morita@yamaguchi-u.ac.jp), [jpshim@kunsan.ac.kr](mailto:jpshim@kunsan.ac.kr)

*Received: 15 March 2016 / Accepted: 3 May 2016 / Published: 4 June 2016*

Sn nanoparticles (NPs) were dispersed on carbon-coated graphite (cG) substrate by the impregnation method using SnCl<sub>2</sub> as the precursor and NaBH<sub>4</sub> as the reducing agent. Sucrose was carbonized to form the coating layer on graphite. The amount of the amorphous carbon-coating layer on the graphite was measured by thermogravimetric analysis. The results of scanning electron microscopy, X-ray diffraction, and inductively coupled plasma atomic emission spectroscopy confirmed the deposition of Sn NPs on the graphite substrate. Sn-deposited materials were electrochemically characterized by charge-discharge cycling. Sn-deposited graphite (Sn/G) showed higher capacity than graphite, and Sn-deposited cG (Sn/cG) showed better electrochemical performance than Sn/G in terms of capacity, coulombic efficiency and cyclability.

**Keywords:** Rechargeable lithium-ion batteries, Sn nanoparticles, Carbon-coated graphite

### 1. INTRODUCTION

Lithium-ion batteries (LIBs) have attracted much attention in the scientific and industrial field as a main power source for portable electronic devices, electric vehicles, etc due to their large electromotive force and high energy density. In recent years, a good deal of attention has been devoted to improving the performance of LIBs by developing better components, including novel electrode materials [1-6]. Graphite and LiCoO<sub>2</sub> are conventionally used for anode and cathode materials due to their stable cycle characteristics, wide potential difference and high theoretical capacity [7-11].

However, development of higher storage capacity devices using graphite anode is limited by the formation of  $\text{LiC}_6$ . For this reason, graphite anodes have been tried to replace by certain metal alloys ( $\text{Li}_x\text{M}$ ,  $\text{M} = \text{Ge}, \text{Si}, \text{Sn}\dots$ ) which have greater theoretical capacity.

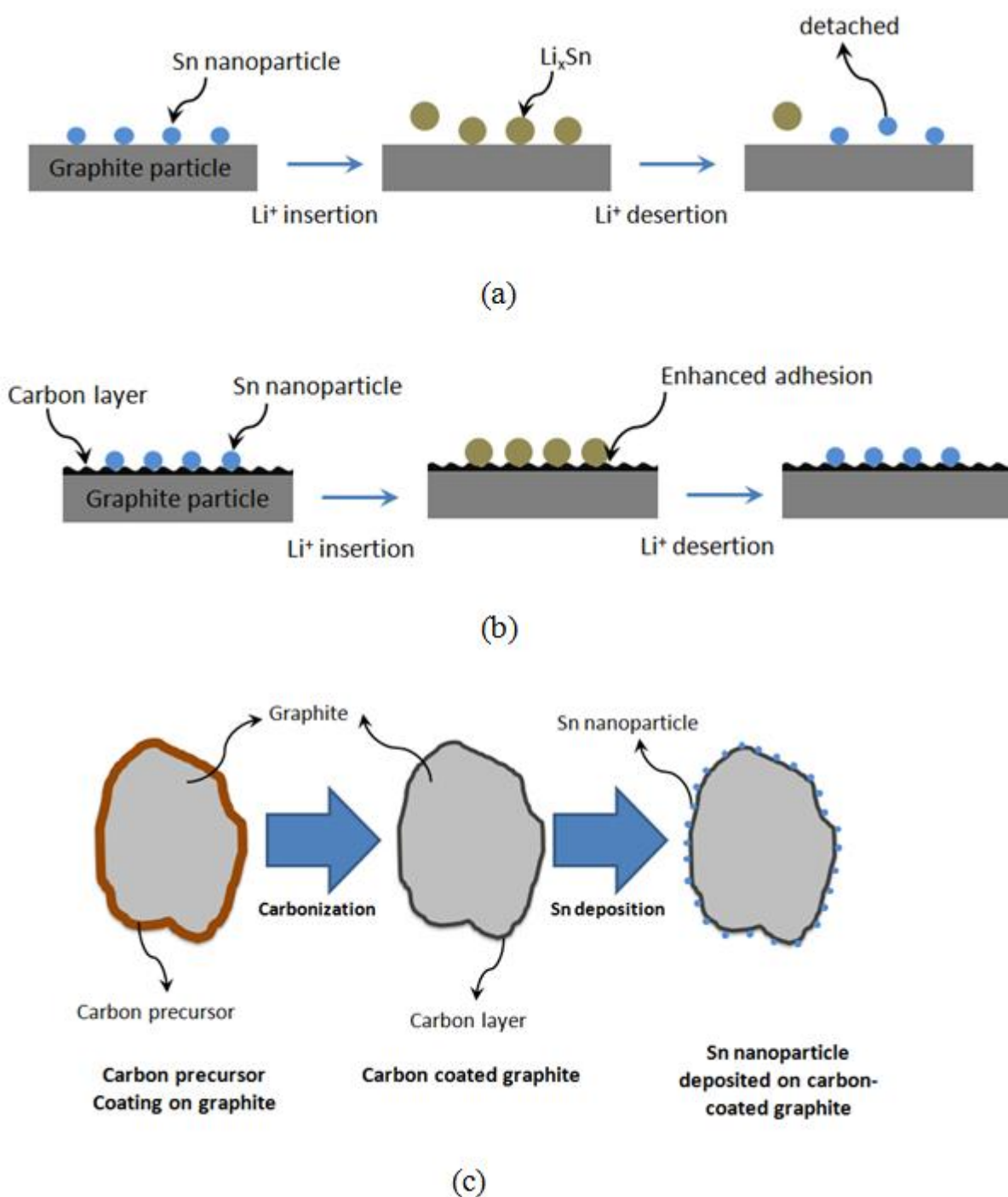


**Figure 1.** Schematic of (a) Sn NP on graphite (Sn/G) composite and improved (b) Sn NP on carbon-coated graphite (Sn/cG) composite for the insertion/desertion of  $\text{Li}^+$  ion, and (c) the preparation progress of Sn/cG

Metallic tin has been widely researched as a promising anode material for LIBs [5,6,12-15]. An equilibrium phase diagram of Li-Sn shows a number of different intermetallic compositions such as

$\text{Li}_5\text{Sn}$ ,  $\text{Li}_{22}\text{Sn}_5$ ,  $\text{Li}_7\text{Sn}_2$ ,  $\text{Li}_3\text{Sn}$ ,  $\text{LiSn}$  and  $\text{Li}_2\text{Sn}_5$ . According to Kamali et al. and Connor et al.,  $\text{Li}_{22}\text{Sn}_5$  possesses specific charge capacity, ~994 mAh/g [5,14]. However, metallic Sn electrodes are cracked and pulverized by the large volumetric variations that occur during the charge and discharge reactions. This mechanical/physical degradation leads to the loss of adhesion and electrical continuity between the electrode and the current collector. This problem has been the biggest stumbling block to the development of practical Sn-based anodes.

In this study, we deposited the tin nanoparticles (Sn NPs) on carbon-coated graphite (cG) composite by chemical reduction. The carbon-coating layer on graphite was prepared by carbonization of organic molecules at 700 °C under inert atmosphere [16]. The effects of Sn NPs and carbon-coating on graphite were investigated in terms of cycling performance by the electrochemical reaction of  $\text{Li}^+$  with Sn. Fig. 1 shows the schematic for the role of carbon-coating layer on graphite. The carbon-coating layer is assumed to enhance the adhesion of Sn NPs to the graphite surface.

The surface area of substrate is the critical factor for maximizing the loading of Sn NPs. If particles are too close, they can agglomerate during charging. The interparticle distance can be theoretically calculated from physical properties of the substrate and the Sn NPs. The BET (Brunauer, Emmett and Teller) surface areas of graphite and cG in this work were 7.55 and 59.17  $\text{m}^2/\text{g}$ , respectively. It was assumed that the average particle sizes of graphite (and cG) and Sn NPs were 20  $\mu\text{m}$  and 20 nm, respectively. The diameter of  $\text{Li}_{4.25}\text{Sn}$  was estimated to be 30.6 nm from the 257% volume expansion of Sn NPs [17]. The number of particles was calculated from the particle size and weight. The interparticle distance was calculated assuming that Sn NPs were located on a flat plane (the surface of substrate). Watanabe et al. have calculated the Pt interparticle distance on carbon black [18,19]; however, we did not use their equation because the interparticle distance was increased after alloying with Li. From these properties, the interparticle distance on the substrates could be calculated as a function of the diameter of Sn NPs, as listed in Table 1. Table 2 shows the variation of interparticle distance on graphite or cG as a function of Sn NPs diameter for 20% Sn loading. For the graphite as substrate, when the diameter of Sn NPs was 20 nm, the calculated distance between  $\text{Li}_{4.25}\text{Sn}$  particles was less than zero. For cG, the calculated interparticle distance of  $\text{Li}_{4.25}\text{Sn}$  was ~45 nm. These calculation are only approximations and do not strictly apply because the surface was assumed to be flat, but in reality the surface area of cG was enlarged by the formation of micropores. But it may be inferred from these calculations that the enlargement of surface area on substrate is an important factor for the deposition of metal NPs.

**Table 1.** Physical properties of materials

	Graphite	Carbon-coated graphite (cG)	Sn NP	$\text{Li}_{4.25}\text{Sn}^{\text{a}}$
Diameter (nm)	20000	20000	20	30.6
Volume ( $\text{mm}^3$ )	$4.19 \times 10^{-6}$	$4.19 \times 10^{-6}$	$3.35 \times 10^{-14}$	$1.20 \times 10^{-13}$
Surface area ( $\text{m}^2/\text{g}$ )	7.55	59.17		

<sup>a</sup> Volume change : 257 % [17]

**Table 2.** Calculation of particle distance on the surface of graphite or carbon-coated graphite (cG) for 20 % Sn loading as a function of Sn particle diameter

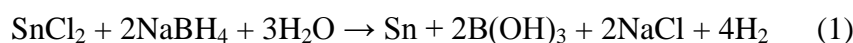
Sn diameter (nm)	Particle distance (nm)			
	Graphite		cG	
	Sn	Li <sub>4.25</sub> Sn	Sn	Li <sub>4.25</sub> Sn
10	-	-	16.7	11.4
20	7.0	-	55.6	45.0
30	19.6	3.8	108.9	93.0
50	56.8	30.3	248.9	222.4

In our earlier papers, we reported that the transition metal chlorides ( $MCl_x$ ) had been reduced and uniformly deposited the metal phase in the form of NPs on the substrate using  $NaBH_4$  as the reducing agent in a conventional impregnation method [20-22]. This could also be achieved by reducing the Sn NPs on cG by simple stirring in solution. These Sn-graphite composite anode materials were characterized in terms of surface morphology and electrochemical behavior by charge-discharge polarization test.

## 2. EXPERIMENTAL

The cG powders were prepared as follows. A mixture of graphite (Posco Chemtech) and sucrose were dispersed and dissolved in water with ethanol. The resulting suspension was heated at 60 °C to evaporate solvent. The obtained powder was heated in a furnace under Argon atmosphere at 700 °C for 2 h during which time, the sucrose was carbonized to form a carbon-coating layer on the surface of graphite powder [23,24].

The Sn-deposited graphite (Sn/G) or cG (Sn/cG) were prepared using  $NaBH_4$  (extra pure, ISHISU Seiyaku Ltd.) as an impregnated method.  $SnCl_2$  (98.0 % Aldrich) as the metal precursor was dissolved in a mixture of water and ethanol. The reduction reaction of  $SnCl_2$  to Sn NPs is as follows [25,26].



The  $NaBH_4$  was added in 5 times excess with respect to  $SnCl_2$  for excluding any residual precursor and thus avoiding side reactions. The graphite or cG substrate was added in 5 mol/cm<sup>3</sup> (mM)  $SnCl_2$  solution and vigorously stirred for 1 h, and then 25 mM  $NaBH_4$  solution was added dropwise into the mixture while stirring. After stirring for 6 h,  $Sn^{2+}$  was completely reduced and impregnated as Sn NPs on the graphite or cG substrate. Finally, the obtained powders were washed 3 times with DI water and were dried at 60 °C for 10 h.

The thermo gravimetric analysis (TGA, Q50, TA instruments) was performed to confirm the ratio of the carbon and graphite in the substrate. The samples were loaded onto low-mass aluminum pans, and measurements were taken from room temperature to 900 °C at a heating rate of 10 °C/min under air. The morphologies of the materials were observed by field-emission scanning electron microscope (FESEM, JSM-7600F, JEOL) with energy-dispersive X-ray spectroscopy (EDS) detector.

The materials were further characterized by X-ray diffraction (XRD, Ultima IV, Rigaku) from  $2\theta = 20 - 80^\circ$  at a rate of  $2^\circ/\text{min}$  using Cu-K $\alpha$  radiation. The content of Sn in the active materials was investigated by inductively coupled plasma atomic emission spectrophotometer (ICP-AES, ICPE-9000, SHIMADZU).

Anodes were fabricated by mixing the active material with carbon black (Super P, Timcal) and poly(vinylidene fluoride) (PVdF, KUREHA) to serve as conductor and binder, in the mass ratio of 85:5:10, respectively. An appropriate amount of 1-methyl-2-pyrrolidone (NMP, 99.0 %, Kanto chemical) solvent in this mixture was needed to achieve a proper consistency for casting. The mixture was cast to control the thickness of  $\sim 130 \mu\text{m}$  on Cu foil ( $20 \mu\text{m}$ , Niraco). These electrodes were dried in vacuum oven at  $120^\circ\text{C}$  for 5 h. The dried electrodes were punched for the same size with 10 mm diameter and pressed at  $300 \text{ kg cm}^{-2}$  to increase the conductivity through improved adhesion between electrode materials and current collector.

For the charge-discharge test, battery-grade  $1.0 \text{ mol/dm}^3$  (M) lithium hexafluorophosphate ( $\text{LiPF}_6$ ) in 1:1 vol% of ethylene carbonate (EC) and dimethyl carbonate (DMC) solution (99.9 %, KANTO chemical) was used as the electrolyte. The electrolyte was used as received without further purification and was stored in an Ar-filled glove box. Electrochemical measurement was performed using a 2-electrode coin-type cell (CR2032, Hoshen). A  $200 \mu\text{m}$  thick Li-ribbon (Honjo Metal Co., Ltd) was used as the counter electrode. A piece of monolayer polypropylene (2500, Celgard) was used as the separator. The electrochemical behaviors of active materials were investigated by the charge-discharge polarization test using a battery cycler (WBCS3000, WonAtech) at ambient temperature. The charge-discharge polarization was normally conducted under a constant current density of  $0.05 \text{ C}$  for activation and  $0.2 \text{ C}$  for cyclability test, in the voltage range of  $0.01 - 1.0 \text{ V}$  (vs.  $\text{Li}/\text{Li}^+$ ). We calculated the C-rate using the theoretical capacity of the Sn and graphite mixture to consider fully activated as  $\text{Li}_{22}\text{Sn}_5$  and  $\text{LiC}_6$ .

### 3. RESULTS AND DISCUSSION

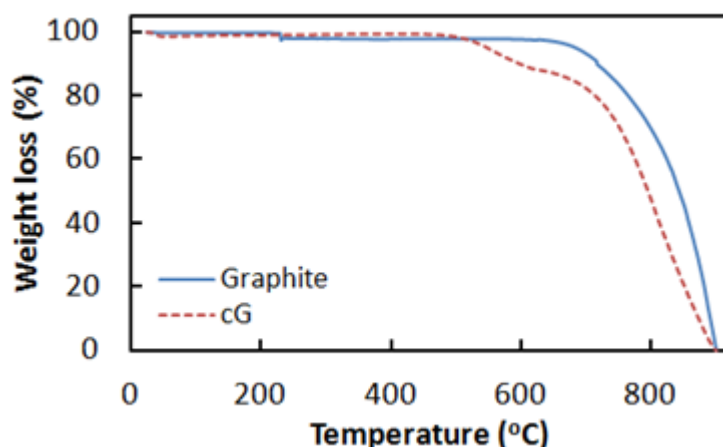


**Figure 2.** TGA curves for graphite and carbon-coated graphite (cG) under air atmosphere

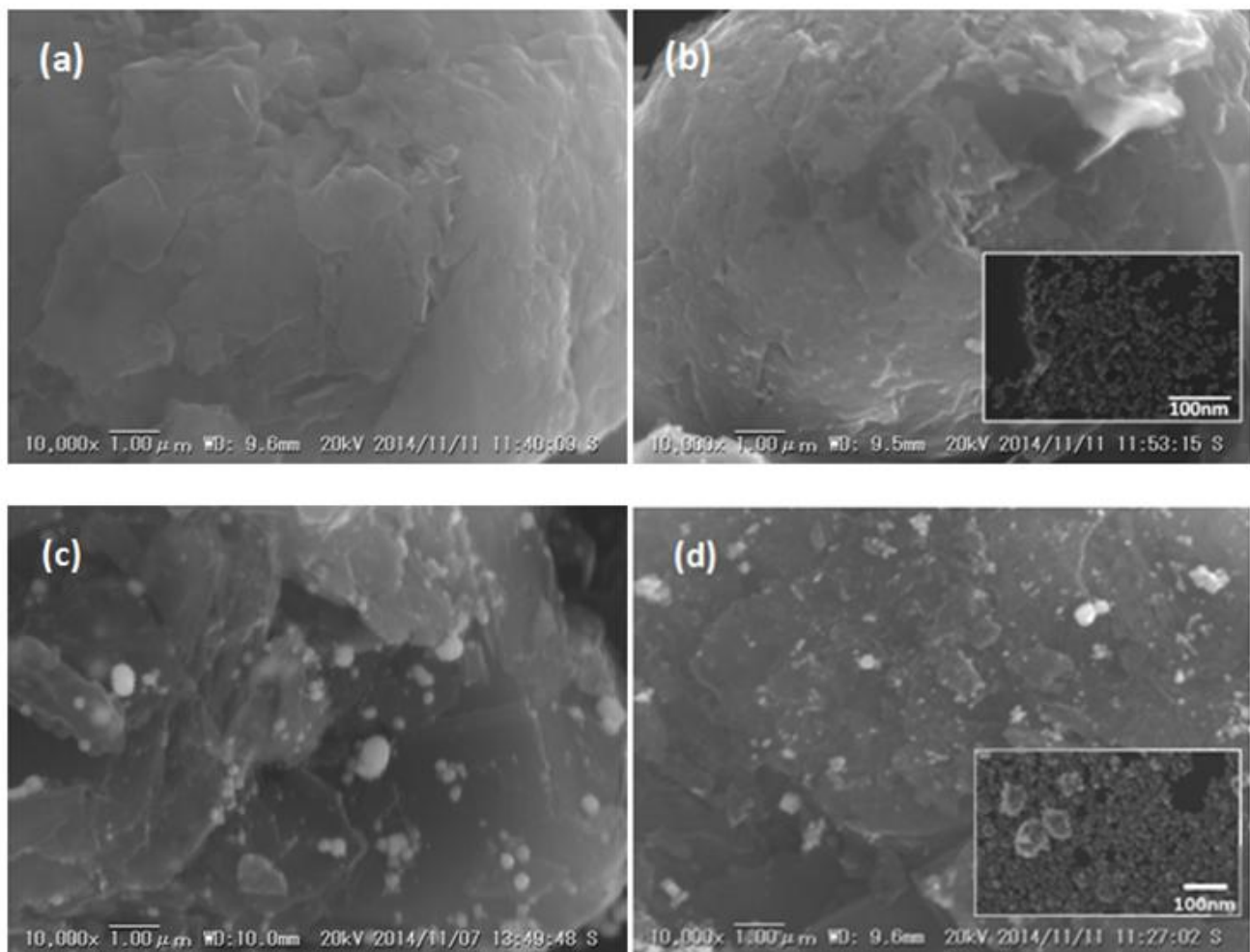


**Figure 3.** SEM images of (a) graphite, (b) cG, (c) Sn/G and (d) Sn/cG.

Fig. 2 shows TGA curves of the graphite and cG as the substrate materials. The graphite substrate showed significant weight loss at 675 °C due to combustion [27]. In contrast, the cG showed a two-step weight loss in the broad temperature range of 450 - 675 °C. It is presumed that the amorphous carbon and graphitic carbon burns at different temperatures in air [28]. The amount of amorphous carbon in cG is ~10.0 wt.%, judging from the TGA result.

The surface morphologies of the materials as observed by SEM are shown in Fig. 3. The inset in Fig. 3 (b) shows that the amorphous carbon was uniformly deposited on the graphite substrate. Fig. 3 (c) and (d) show Sn NPs, having sizes of tens to hundreds of nanometer, were well dispersed on graphite or cG substrate. The inset in Fig. 3 (d) shows that the amorphous carbon could also be uniformly deposited. ICP-AES results confirmed that the amounts of Sn NPs in Sn/G and Sn/cG were ~24 and ~27 wt%, respectively. In addition, better distribution of Sn NPs was found on cG, which has a substantially larger surface area than graphite.

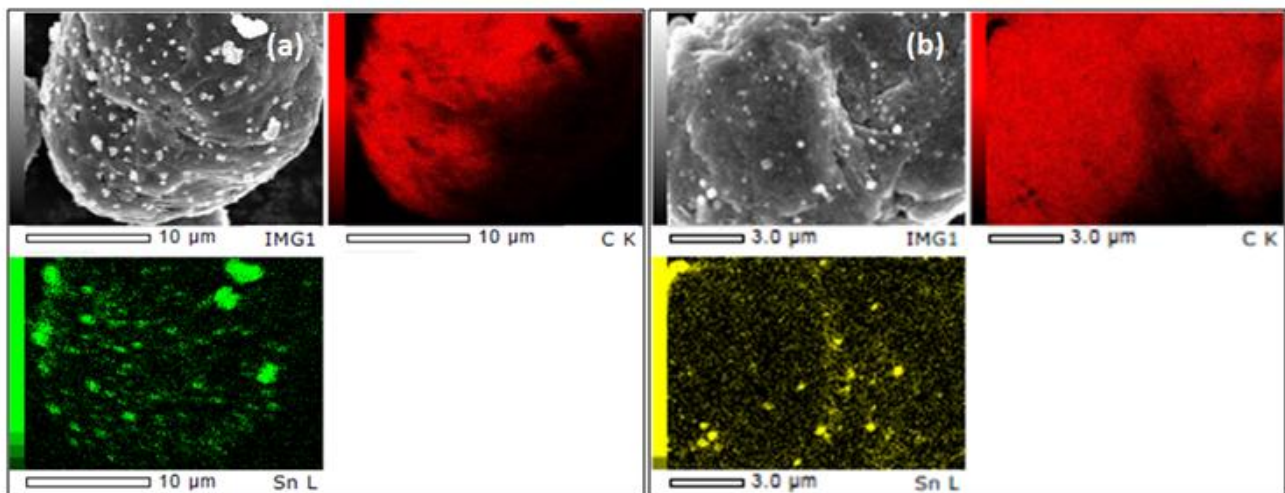


**Figure 4.** EDS mapping of (a) Sn/G and (b) Sn/cG

Elemental mapping for Sn shows uniform distribution on graphite or cG in Fig. 4, and that Sn NPs are better distributed on cG, which is in agreement with Fig. 3.

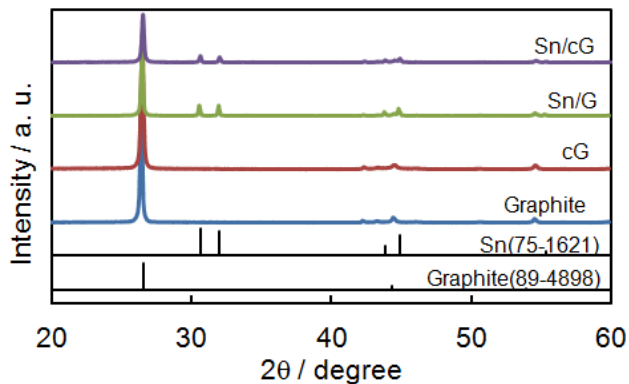


**Figure 5.** XRD patterns of graphite, cG, Sn/G and Sn/cG active materials

Fig. 5 shows XRD patterns of the active materials and original patterns of graphite and Sn from JCPDS file (89-4898 and 75-1621). The main diffraction peaks of  $30.6^\circ$ ,  $32.0^\circ$ ,  $43.9^\circ$ ,  $44.9^\circ$  and  $55.3^\circ$  are assigned to metallic Sn, and those at  $26.6^\circ$ ,  $44.3^\circ$  and  $54.5^\circ$  to the graphite substrate. The XRD pattern of Sn/G and Sn/cG clearly substantiated the existence of Sn NPs on the substrate. The average crystallite sizes of graphite (002), calculated by Scherrer equation, were 23.9 nm and 26.3 nm for the graphite and cG substrates, respectively. The slight increase in crystallite size for the (002) plane may be induced by the carbon-coating layer on graphite because of the overlap of the amorphous carbon peak [29]. The crystallite sizes of Sn, which were calculated using the diffraction peak of  $30.6^\circ$  for the Sn (200) plane, were 48.4 nm and 45.7 nm in Sn/G and Sn/cG, respectively. The SEM and XRD

results show that the carbon-coating on graphite produce an active material with smaller particle size and better dispersed Sn on the substrate.

Fig. 6 shows the first and second cycles of charge-discharge for the active materials. Graphite showed discharge capacities of 370 and 375 mAh/g for the first and second cycles, which are close to the theoretical capacity. In comparison, cG showed slightly increased capacities of 383 and 390 mAh/g because the amorphous carbon coating could accept a small amount of  $\text{Li}^+$  ion [30]. In contrast, when Sn NPs were deposited on graphite or cG, the discharge capacities were significantly increased. Sn/G and Sn/cG showed 478/477 and 496/497 mAh/g of discharge capacities for the first and second cycles, which were ~26 and 30% of increased values, respectively. Sn-deposited materials were showing another plateau around 0.5 V, comparing with graphite.

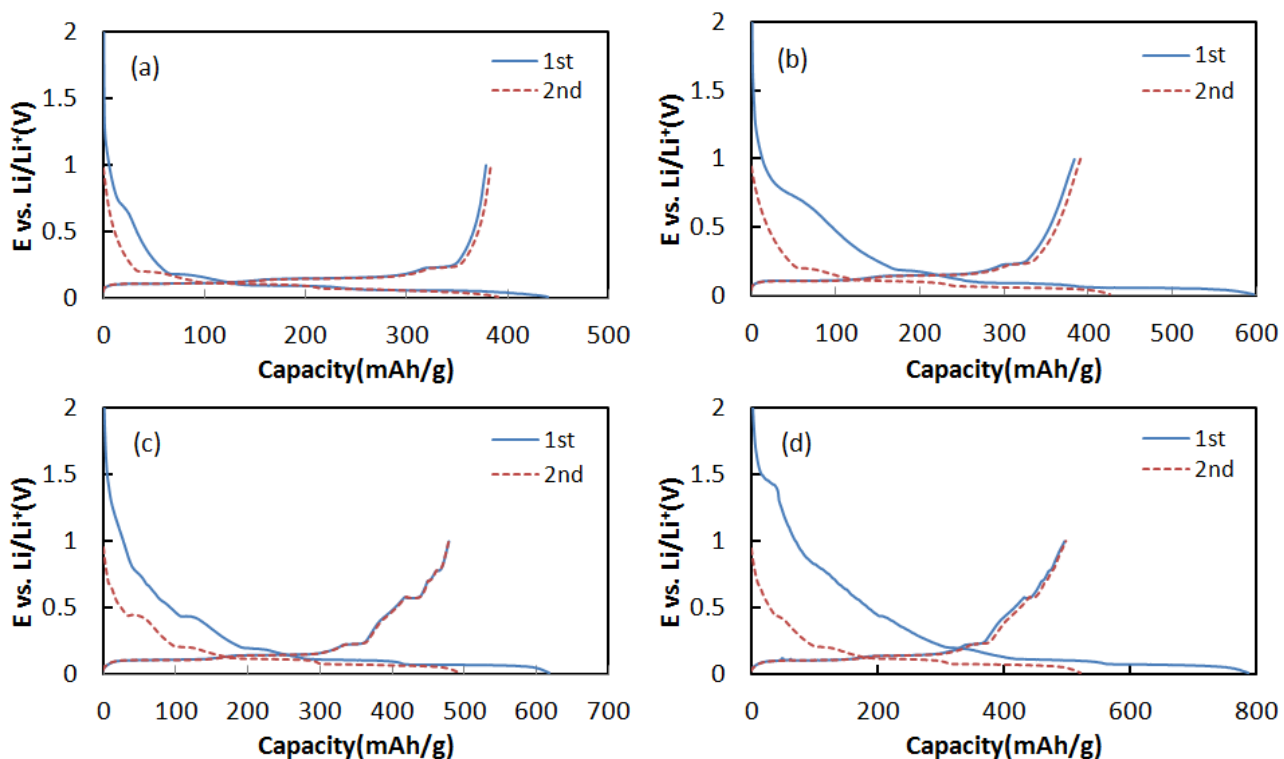


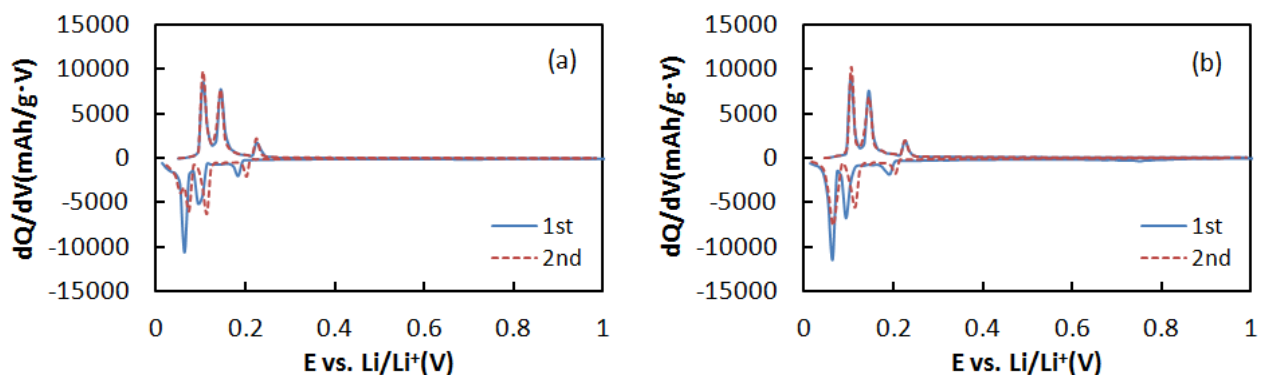
**Figure 6.** Charge-discharge polarization curves of (a) graphite, (b) cG, (c) Sn/G and (d) Sn/cG electrodes at 0.1 C rate in 1.0 M  $\text{LiPF}_6/\text{EC+DMC}$ (1:1 vol.%) electrolyte

Capacities and efficiencies for the two initial cycles are listed in Table 3. Original graphite had irreversible capacity losses of 13.7% and 4.0% of at the first and second cycles, respectively. This was increased to 35.7% at the first cycle by carbon-coating. Sn/G and Sn/cG had irreversible capacity losses of 31.7% and 37.0% at the first cycle. Sn/G still had 13.5% irreversible capacity loss at the second cycle but that of Sn/cG was lowered to 4.6%, which was close to that of original graphite. Irreversible capacities of Sn reported in the literature are around 20-40% at initial cycles (Table 3).

**Table 3.** Capacities and efficiencies of active materials at 1<sup>st</sup> and 2<sup>nd</sup> cycles

Materials	1 <sup>st</sup> cycle			2 <sup>nd</sup> cycle			Ref.
	Chg. Cap. (mAh/g)	Dchg. Cap. (mAh/g)	Eff. (%)	Chg. Cap. (mAh/g)	Dchg. Cap. (mAh/g)	Eff. (%)	
Graphite	440.1	370.9	84.3	391.1	375.3	96.0	
cG	595.8	383.1	64.3	424.9	390.3	91.9	Present works
Sn/G	616.8	478.1	68.3	492.9	477.6	86.5	
Sn/cG	786.5	495.6	63.0	519.7	496.8	95.6	
Sn/MCMB	543.1	422.0	77.7		434.8		[31]
Sn/C	~1580	~520	~33	~630	~530	~84	[32]
Sn/hard carbon	580	440	75.9				[33]
SnSb/MCMB/carbon	554.3	487.3	83.5				[34]
Sn/SnO <sub>x</sub> /carbon nanofiber	1192	457	61.7				[35]

dQ/dV plots in Fig. 7 shows clear evidence of intercalation/deintercalation or alloying of Li<sup>+</sup> ion with graphite and Sn, respectively. Graphite showed typical peaks for the intercalation/deintercalation between graphene layers [36,37]. cG had another tiny peak around 0.77 V, which was attributed to greater electrolyte decomposition on porous carbon layer [38]. Electrochemical alloying of Sn with Li has several potential plateaus around 0.38, 0.42, 0.45, 0.53, and 0.66 V for forming Li<sub>3.5-4.4</sub>Sn, Li<sub>2.6-3.5</sub>Sn, Li<sub>2.3-2.6</sub>Sn, Li<sub>0.7-2.3</sub>Sn, and Li<sub>0.4-0.7</sub>Sn, respectively [39,40]. Insets in Fig. 7 (c) and (d) show that Sn/G and Sn/cG had peaks around 0.44, 0.55 and 0.67 V for alloying with Li. These three peaks may be assigned to the formation of Li<sub>2.3-3.5</sub>Sn, Li<sub>0.7-2.3</sub>Sn, and Li<sub>0.4-0.7</sub>Sn. The peak around 0.38 V, which was correlated to the formation of Li<sub>3.5-4.4</sub>Sn in the literature, was not found in our results. This means Li<sup>+</sup> was not inserted to final stage of Li-Sn alloying, and their capacities could not reach to theoretical one. Moreover, these materials had corresponding plateaus for dealloying which were shifted to higher potentials of 0.11-0.15 V. From Fig. 7, it was observed that Sn deposited on graphite or cG could react with Li independently, which was not affected by graphite as supporter.



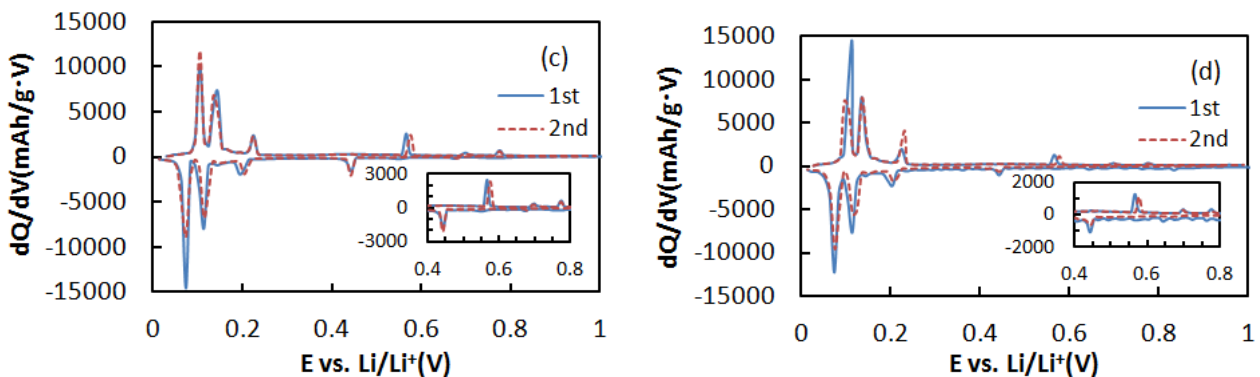


**Figure 7.**  $dQ/dV$  plots of (a) graphite, (b) cG, (c) Sn/G and (d) Sn/cG electrodes for 1<sup>st</sup> and 2<sup>nd</sup> cycles at 0.05 C rate.

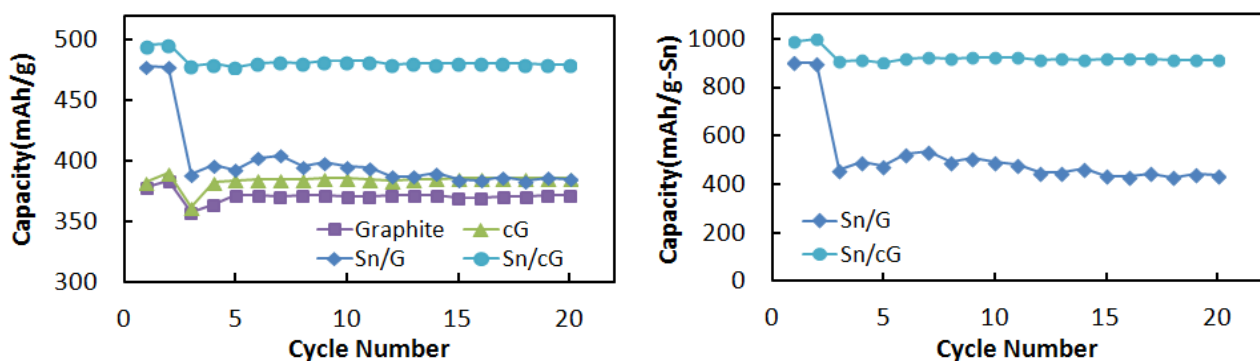


**Figure 8.** Specific discharge capacity of graphite, cG, Sn/G and Sn/cG electrodes per amount of (a) active material and (b) Sn as a function of cycle numbers. 0.05 C at first 2 cycles and 0.2C for the rest cycles

Fig. 8 (a) shows the cycle performances for four materials, and the capacities in Fig. 8 (b) were calculated from the weights of Sn obtained after subtracting the capacity of graphite (assuming 372 mAh/g). Most materials showed stable capacity retention up to 20 cycles. Capacities of Sn/G and Sn/cG during continuous cycling at 0.2 C were ~390 and ~480 mAh/g, respectively. Capacity fading rates of graphite and cG were 40.7 and 55.3  $\mu\text{Ah/g}\cdot\text{cycle}$ , respectively. Sn/G showed a capacity fading rate of 1188.8  $\mu\text{Ah/g}\cdot\text{cycle}$ , which was 21.5 and 29.2 times higher than those of graphite and cG, respectively. However, the capacity fading rate of Sn/cG sharply decreased to 52.4  $\mu\text{Ah/g}\cdot\text{cycle}$ . As shown in Fig. 8 (b), the capacities of Sn in Sn/G were 450–500 mAh/g-Sn which was lower than the theoretical capacity of Sn (994 mAh/g). However, Sn in Sn/cG showed a capacity of ~910 mAh/g-Sn, which was ~90 % of the theoretical capacity. We have not found any report on the capacity of Sn reaching ~90 % of the theoretical capacity in the range of 0.01–1.0 V (vs.  $\text{Li}/\text{Li}^+$ ) [41,42]. The capacity of Sn in Sn/cG was still over 900 mAh/g-Sn after the 20<sup>th</sup> cycle with a capacity fading rate of 26.0  $\mu\text{Ah/g}\cdot\text{Sn}\cdot\text{cycle}$ . These results indicate that Sn-deposited graphite anode materials, which had stable cyclability and ~30 % higher capacity than graphite, could be successfully synthesized by a simple

chemical reduction process at room temperature without any heat-treatment [43,44] and physical deposition [45,46].

#### 4. CONCLUSION

The Sn-deposited on graphite or carbon-coated graphite (cG) were successfully synthesized by a simple chemical reduction process at room temperature. The deposition of Sn NPs on substrates was confirmed by XRD, SEM, and ICP-AES. The distribution of Sn NPs on cG was more uniform and their sizes were smaller than those on graphite because of larger surface area. Sn/G and Sn/cG showed reversible capacities of 478.1 and 495.6 mAh/g at the first cycle, respectively, which were higher than that of graphite (370.9 mAh/g). Correspondingly, their efficiencies were 68.3 and 63.0%, which were lower than that of graphite (84.3%). However, the efficiency of Sn/cG at the second cycle recovered to 95.6%. Sn/cG showed very stable cyclability, and its capacity reached ~90 % of the theoretical capacity during continuous cycling at a rate of 0.2 C. The amorphous carbon layer on the graphite may enhance the adhesion of Sn NPs by compensating for the volumetric expansion during the alloying/dealloying with Li.

#### ACKNOWLEDGEMENT

This research was supported by the Ministry of Trade, Industry & Energy (MOTIE), Korea Institute for Advancement of Technology (KIAT) through the Encouragement Program for The Industries of Economic Cooperation Region.

#### References

1. Z. X. Shu, R. S. Mcmillian, J. J. Murray and I. J. Davidson, *J. Electrochem. Soc.*, 143 (1996) 2230.
2. G. Derrien, J. Hassoun, S. Panero and B. Scrosati, *Adv. Mater.*, 19 (2007) 2336.
3. M. Armand and J.-M. Tarascon, *Nature*, 451 (2008) 652.
4. I. D. Scott, Y. S. Jung, A. S. Cavanagh, Y. Yan, A. C. Dillon, S. M. George and S.-H. Lee, *Nano Lett.*, 11 (2011) 414.
5. A. R. Kamali and D. J. Fray, *Rev. Adv. Mater. Sci.*, 27 (2011) 14.
6. W.-M. Zhang, J.-S. Hu, Y.-G. Guo, S.-F. Zheng, L.-S. Zhong, W.-G. Song and L.-J. Wan, *Adv. Mater.*, 20 (2008) 1160.
7. B. Huang, Y.-I. Jang, Y.-M. Chiang and D. R. Sadoway, *J. Appl. Electrochem.*, 28 (1998) 1365.
8. R. A. Leising, M. J. Pallazzo, E. S. Takeuchi and K. J. Takeuchi, *J. Electrochem. Soc.*, 148 (2001) A838.
9. S.-K. Jeong, M. Inaba, R. Mogi, Y. Iriyama, T. Abe and Z. Ogumi, *Langmuir*, 17 (2001) 8281.
10. J. Shim and K. A. Striebel, *J. Power Sources*, 119-121 (2003) 934.
11. K. A. Striebel, A. Sierra, J. Shim, C.-W. Wang and A. M. Sastry, *J. Power Sources*, 134 (2004) 241.
12. B. Scrosati, *Electrochim. Acta*, 45 (2000) 2461.
13. G. X. Wang, J.-H. Ahn, M. J. Lindsay, L. Sun, D. H. Bradhurst, S. X. Dou and H. K. Liu, *J. Power Sources*, 97-98 (2001) 211.
14. P. A. Connor and J.T.S. Irvine, *J. Power Sources*, 97-98 (2001) 223.

15. T. Morishita, T. Hirabayashi, T. Okuni, N. Ota and M. Inagaki, *J. Power Sources*, 160 (2006) 638.
16. H. Lia and H. Zhou, *Chem. Comm.*, 48 (2012) 1201.
17. G.A. Nazri and G. Pistoia, "Lithium batteries, Science and technology", Kluwer Academic Publishers, 2004, p117
18. M. Watanabe, H. Sei and P. Stonehart, *J. Electroanal. Chem.*, 261 (1989) 375.
19. M. Watanabe, S. Saegusa and P. Stonehart, *Chem. Lett.*, 17 (1988) 1487.
20. I.-T. Kim, H.-K. Lee and J. Shim, *J. Nanosci. Nanotech.*, 8 (2008) 5302.
21. I.-T. Kim, M. Choi, J.-C. An, H.-K. Lee and J. Shim, *J. Nanosci. Nanotech.*, 10 (2010) 3643.
22. M. Choi, C. Han, I.-T. Kim, J.-C. An, J.-J. Lee, H.-K. Lee and J. Shim, *J. Nanosci. Nanotech.*, 11 (2011) 838.
23. N. Ravet, Y. Chouinard, J.F. Magnan, S. Besner, M. Gauthier and M. Armand, *J. Power Sources*, 97-98 (2011) 503.
24. H. Wang, M. Yoshio, T. Abe and Z. Ogumi, *J. Electrochem. Soc.*, 149 (2002) A499.
25. W.-S. Seo, T.-H. Kim, J.-S. Sung and K.-C. Song, *Korean Chem. Eng. Res.*, 42 (2004) 78.
26. K. Torigoe, Y. Nakajima, and K. Esumi, *J. Phys. Chem.*, 97 (1993) 8304.
27. J. Lee, S. Won, J. Shim, G. Park, H.-J. Sun and H.-K. Lee, *Trans. Electr. Electron. Mater.*, 15 (2014) 193.
28. S. Osswald, G. Yushin, V. Mochalin, S. O. Kucheyev and Y. Gogotsi, *J. Am. Chem. Soc.*, 128 (2006) 11635.
29. Y.-S. Park, H.J. Bang, S.-M. Oh, Y.-K. Sun and S.-M. Lee, *J. Power Sources*, 190 (2009) 553.
30. L Fransson, T. Eriksson, K. Edström, T. Gustafsson and J.O. Thomas, *J. Power Sources*, 101 (2001) 1.
31. M.-J. Denga, D.-C. Tsai, W.-H. Ho, C.-F. Li and F.-S. Shieu, *Appl. Surf. Sci.*, 285 (2013) 180.
32. C. Nabais, R. Schneider, P. Willmann and D. Billaud, *Energy Conv. Manag.*, 56 (2012) 32.
33. B. Guo, J. Shu, K. Tang, Y. Bai, Z. Wang and L. Chen, *J. Power Sources*, 177 (2008) 205.
34. J. Li, Q. Ru, S. Hu, D. Sun, B. Zhang and X. Hou, *Electrochim. Acta*, 113 (2013) 505.
35. L. Zou, L. Gan, R. Lv, M. Wang, Z.-h. Huang, F. Kang and W. Shen, *Carbon*, 49 (2011) 89.
36. T. Ohzuku, Y. Iwakoshi and K. Sawai, *J. Electrochem. Soc.*, 140 (1993) 2490.
37. J. Shim and K.A. Striebel, *J. Power Sources*, 130 (2004) 247.
38. H. Wang and M. Yoshio, *J. Power Sources*, 93 (2001) 123.
39. J. Wang, I.D. Raistrick and R.A. Huggins, *J. Electrochem. Soc.*, 133 (1986) 457.
40. R.A. Huggins, *J. Power Sources*, 26 (1989) 109.
41. Y. Xu, Q. Liu, Y. Zhu, Y. Liu, A. Langrock, M.R. Zachariah and C. Wang, *Nano Lett.*, 13 (2013) 470.
42. B. Luo, B. Wang, X. Li, Y. Jia, M. Liang and L. Zhi, *Adv. Mater.*, 24 (2012) 3538.
43. G. Wang, Y.Q. Ma, Z.Y. Liu and J.N. Wu, *Electrochim. Acta*, 65 (2012) 275.
44. L. Liu, M. An, P. Yang and J. Zhang, *Int. J. Electrochem. Sci.*, 10 (2015) 4461.
45. W. Liu, S. Zhang, N. Li, S. An, and J. Zheng, *Int. J. Electrochem. Sci.*, 8 (2013) 347.
46. F. Nobili, M. Mancini, P.E. Stallworth, F. Crocec, S.G. Greenbaum and R. Marassia, *J. Power Sources*, 198 (2012) 243.